
Double Bubble, Toil and Trouble: Enhancing Certified Robustness through Transitivity

Andrew C. Cullen^{1*} Paul Montague² Shijie Liu¹
 Sarah M. Erfani¹ Benjamin I.P. Rubinstein¹

¹School of Computing and Information Systems, University of Melbourne, Parkville, Australia

²Defence Science and Technology Group, Adelaide, Australia

andrew.cullen@unimelb.edu.au

Abstract

In response to subtle adversarial examples flipping classifications of neural network models, recent research has promoted certified robustness as a solution. There, invariance of predictions to all norm-bounded attacks is achieved through randomised smoothing of network inputs. Today’s state-of-the-art certifications make optimal use of the class output scores at the input instance under test: no better radius of certification (under the L_2 norm) is possible given only these scores. However, it is an open question as to whether such *lower bounds* can be improved using local information around the instance under test. In this work, we demonstrate how today’s “optimal” certificates can be improved by exploiting both the transitivity of certifications, and the geometry of the input space, giving rise to what we term *Geometrically-Informed Certified Robustness*. By considering the smallest distance to points on the boundary of a set of certifications this approach improves certifications for more than 80% of Tiny-Imagenet instances, yielding an on average 5% increase in the associated certification. When incorporating training time processes that enhance the certified radius, our technique shows even more promising results, with a uniform 4 percentage point increase in the achieved certified radius.

1 Introduction

Learned models, including neural networks, are well known to be susceptible to having the output changed by crafted perturbations to an input, that preserve the input’s semantic properties [2]. Neural networks not only misclassify these perturbations—known as *adversarial examples*—but they also assign high confidence to these incorrect predictions. These behaviours have been observed across a wide range of models and datasets, and appear to be a product of piecewise-linear interactions [13].

Crafting these adversarial examples typically involves gradient-based optimisation to construct *small* perturbations. These attacks have been applied to both black- and white-box models [31], and can be used to target class changes, to attack all classes [10], or even introduce backdoors into model behaviour [5]. To mitigate the influence of these attacks, defences have typically been designed to minimise the effect of a specific attack (or attacks). Such defences are known as *best response* strategies in a Stackelberg security game where the defender leads the attacker. Best response defences inherently favour the attacker, as deployed mitigations can be defeated by identifying undefended attack frameworks. Moreover, the defender typically has to incorporate the defence at training time, and as such cannot respond reactively to newly developed attacks.

To circumvent these limitations, certified guarantees of adversarial robustness can be constructed to identify class-constant regions around an input instance, that guarantee that all instances within a norm-bounded distance (typically L_2) are not adversarial examples. Certifications based on randomised smoothing of classifiers around an input point are in a sense optimal [8]: based only on the prediction

class scores at the input point, no better radius is in general possible. Despite this, such certifications fail to use readily available—yet still local—information: the certifiability of points nearby to the input of interest. The key insight of this work is that these neighbourhood points may generate certified radius large enough to completely enclose that of a sample point, improving the radius of certification. This process can be extended to use the intersection of the regions of certification of multiple points, and the nature of the input domain itself to generate larger certifications. This leads to our main contribution—*Geometrically-Informed Certified Robustness*—that enjoys certifications exceeding those of the hitherto best-case guaranteed approach of Cohen *et al.* (2019) [8].

2 Background and literature review

Bounding mechanisms Conservative bounds upon the impact of norm-bounded perturbations can be constructed by way of either Interval Bound Propagation (IBP) which propagates interval bounds through the model; or Convex Relaxation, which utilise linear relaxation to construct bounding output polytopes over input bounded perturbations [34, 26, 41, 45, 46, 37, 28], in a manner that generally provides tighter bounds than IBP [25]. In contrast to Randomised Smoothing, bounding mechanisms employ augmented loss functions during training, which promote tight output bounds [42] at the cost of decreased applicability. Moreover they both exhibit a time and memory complexity that makes them infeasible for complex model architectures or high-dimensional data [40, 6, 21].

Randomised smoothing Outside of bounding mechanisms, another common framework for developing certifications leverages *randomised smoothing* [20], in which noise is applied to input instances to smooth model predictions, subject to a sampling distribution that is tied to the L_P -norm of adversarial perturbations being certified against. In contrast to other robustness mechanisms, this application of the noise is the only architectural change that is required to achieve certification. In the case of L_2 -norm bounded attacks, Gaussian sampling of the form

$$\mathbf{x}'_i = \mathbf{x} + \mathbf{y}_i \quad \text{where } \mathbf{y}_i \stackrel{i.i.d.}{\sim} \mathcal{N}(0, \sigma^2) \quad \forall i \in \{1, \dots, N\} \quad (1)$$

is employed for all test-time instances. These N samples are then used to estimate the expected output of the predicted class of \mathbf{x} by way of the Monte-Carlo estimator

$$E_{\mathbf{Y}}[\arg \max f_{\theta}(\mathbf{x} + \mathbf{Y}) = i] \approx \frac{1}{N} \sum_{j=1}^N \mathbb{1}[\arg \max f_{\theta}(\mathbf{x}_j) = i] . \quad (2)$$

While this Monte Carlo estimation of output expectations under randomised smoothing is a test-time process, model sensitivity to random perturbations may be decreased by performing adversarial training on such random perturbations. To mitigate the computational expense of large N sample sizes during each training update, training typically employs single draws from the noise distribution.

Smoothing-based certifications Based on randomised smoothing, certified robustness can guarantee classification invariance for *additive* perturbations up to some L_p -norm r , with recent work also considering rotational and/or translational semantic attacks [23, 7]. L_p -norm certifications were first demonstrated by way of differential privacy [20, 11], with more recent approaches employing Rényi divergence [22], and parametrising worst-case behaviours [8, 33]. By considering the worst-case L_2 -perturbations, Cohen *et al.* (2019) purports that the largest achievable pointwise certification is

$$r = \frac{\sigma}{2} (\Phi^{-1}(E_0[\mathbf{x}]) - \Phi^{-1}(E_1[\mathbf{x}])) . \quad (3)$$

Here $\{E_0, E_1\}$ are the two largest class expectations (as per Equation (2)), σ is the noise, and Φ^{-1} is the inverse normal CDF, or Gaussian quantile function.

3 Geometrically-informed certified robustness

While the work contained within this paper can be applied generally, for this work we will focus upon certifications of robustness about L_2 -norm bounded adversarial perturbations, for which we assume that the difficulty of attacking a model is proportional to the size of the certification, based upon the need to evade both human *and* machine scrutiny [12]. Thus, constructing larger certifications in such a context is inherently valuable.

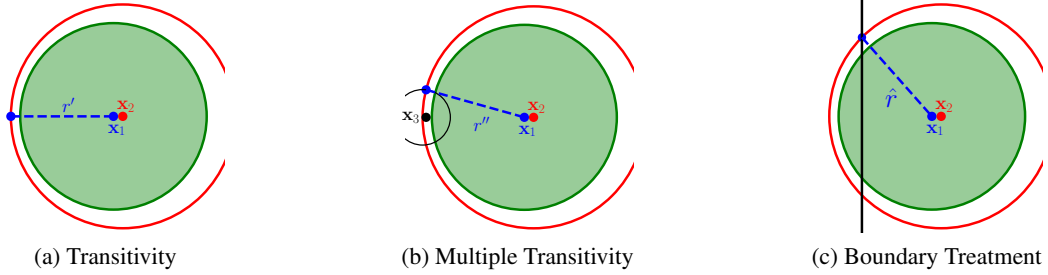


Figure 1: Transitive certification exemplars. The Green, Red, and Black circles represent hyperspheres of radius r_i (by Equation 3) about points $\mathbf{x}_i \forall i \in \{1, 2, 3\}$. The resulting certifications r' , r'' , and \hat{r} are described within Equations 5, 12, and 16. The Black line represents the domain boundary.

This specific L_P space is of interest due to both its viability as a defence model, and the provable guarantee that Cohen *et al.* produces the largest possible certification for any instance [8]. Over the remainder of this section we will document how it is possible to improve upon this provably best-case guarantee by exploiting several properties of certified robustness.

3.1 Exploiting transitivity

While it is provably true that Equation (3) is the largest achievable certification for any point \mathbf{x} , it is possible to exploit the behaviour of points in the neighbourhood of \mathbf{x} in order to enhance certifiable radius. To achieve this, consider the case of a second point \mathbf{x}' , that exists within the certifiable radius of \mathbf{x} . As both points must correspond to the same class, it then follows that the union of their regions of certification can be also be considered as a region of certification, leading to Definition 3.1.

Definition 3.1 (Overlap Properties of Certification). A radius of certification r_i about \mathbf{x}_i can be calculated by evaluating Equation 3 at \mathbf{x}_i . This certification guarantees that no point $\mathbf{x} : \|\mathbf{x} - \mathbf{x}_i\|_P \leq r_i$ can induce a chance in the predicted class. That this shape is a d -dimensional hypersphere for input data $\mathbf{x} \in \mathcal{R}^d$ allows us to introduce the notational shorthand

$$B_P(\mathbf{x}_i, r_i) = \{\mathbf{x} \in \mathcal{R}^d \mid \|\mathbf{x} - \mathbf{x}_i\|_P \leq r_i\} \quad S_i = \{\mathbf{x} \in \mathcal{R}^d \mid \|\mathbf{x} - \mathbf{x}_i\|_P = r_i\} \quad (4)$$

to represent the region covered by the hypersphere and its surface. It follows from this definition that that if $B_P(\mathbf{x}_1, r_1) \cap B_P(\mathbf{x}_2, r_2) \neq \emptyset$, which ensures that the class predictions at \mathbf{x}_1 and \mathbf{x}_2 match, then the region of certification about \mathbf{x}_1 can be expressed as $B_P(\mathbf{x}_1, r_1) \cup B_P(\mathbf{x}_2, r_2)$.

However typically we are concerned not with the size of the region of classification invariance, but rather the distance to the nearest adversarial example. If it is possible to find some \mathbf{x}' such that its region of certification completely encircles that of the certification at \mathbf{x} , the following definition demonstrates that the certification radius about \mathbf{x} can be increased.

Lemma 3.2 (Set Unions Certified Radius). If \mathbf{x}_1 and \mathbf{x}_2 have the same class associated with them and $B_P(\mathbf{x}_1, r_1) \subset B_P(\mathbf{x}_2, r_2)$, then the nearest possible adversarial example—and thus, the certifiable radius—exists at a distance $r' \geq r$ from \mathbf{x}_1 , where

$$r' = r_2 - \|\mathbf{x}_2 - \mathbf{x}_1\|_P, \quad (5)$$

Proof. The closest point on the surface of $B_P(\mathbf{x}_2, r_2)$ to \mathbf{x}_1 must exist on the vector between \mathbf{x}_1 and \mathbf{x}_2 . Thus $r' = \min(r_2 \pm \|\mathbf{x}_2 - \mathbf{x}_1\|_P)$, which takes the form of Equation (5). \square

As such, we can recast the task of constructing a certification from being a strictly analytic function to the nonlinear optimisation problem in terms of a second ball with certified radius r_2 centred at \mathbf{x}_2

$$r' = \max_{\mathbf{x}_2 \in [0,1]^d} r_2 - \|\mathbf{x}_2 - \mathbf{x}_1\|_P \quad (6)$$

with Figure 1a providing a two-dimensional exemplar. Crucially, the above formalism does not require obtaining a global optima, as any $r' > r_1$ yields an improved certification at \mathbf{x}_1 .

3.2 Multiple transitivity

To further enhance our ability to certify, let us consider the set of points and their associated certifications $\{\mathbf{x}_1, r_1, \mathbf{x}_2, r_2, \dots, \mathbf{x}_n, r_n\}$. If the union of $\hat{B}_P = \bigcup_{i \in \{1, \dots, n\}} B_P(\mathbf{x}_i, r_i)$ is simply-connected, then the certification across this set can be expressed as $r^{(n)'} = \min_{\mathbf{x} \in \partial \hat{B}_P} \|\mathbf{x} - \mathbf{x}_1\|_P$, where $\partial \hat{B}_P$ is the boundary of \hat{B}_P . This can be further simplified by imposing that $\mathbf{x}_j \in B_P(\mathbf{x}_2, r_2) \forall j > 2$ and that $B_P(\mathbf{x}_j, r_j) \not\subset B_P(\mathbf{x}_k, r_k) \forall (j > 2, k > 2)$ to ensure that hyperspheres exist near the boundary of \mathcal{S}_2 and yielding a certification of

$$r^{(n)'} = \min_{\mathbf{x} \in \mathbf{S}_n} \|\mathbf{x} - \mathbf{x}_1\| \text{ where } \mathbf{S}_n = \mathcal{S}_2 \cap (\cup_{i=3}^{n+1} S_i) \text{ for } n \geq 2 . \quad (7)$$

Here \mathbf{S}_n is a $(d-1)$ -dimensional manifold embedded in \mathcal{R}^d .

Lemma 3.3 (Optimal positioning of \mathbf{x}_3 in the case of $n = 3$). *Consider the addition of a new hypersphere at some point \mathbf{x}_3 with associated radius r_3 , which has an associated boundary \mathcal{S}_3 . If it is true that*

$$B_P(\mathbf{x}_3, r_3) \not\subset B_P(\mathbf{x}_2, r_2) \text{ and } B_P(\mathbf{x}_3, r_3) \cap B_P(\mathbf{x}_2, r_2) \neq \emptyset \quad (8)$$

$$B_P(\mathbf{x}_3, r_3) \not\subset B_P(\tilde{\mathbf{x}}, \tilde{r}) \forall \{\tilde{\mathbf{x}} \in [0, 1]^d | \tilde{\mathbf{x}} \neq \mathbf{x}_3\} \text{ with } \tilde{r} = \frac{\sigma}{2} (\Phi^{-1}(E_0[\tilde{\mathbf{x}}]) - \Phi^{-1}(E_1[\tilde{\mathbf{x}}])) , \quad (9)$$

then the largest possible certification r'' by Equation 7 is achieved at

$$\mathbf{x}_3(s) = \mathbf{x}_1 + sr' \frac{\mathbf{x}_1 - \mathbf{x}_2}{\|\mathbf{x}_1 - \mathbf{x}_2\|_2} \quad \text{for some } s \in [0, 1] . \quad (10)$$

Proof. The closest point to \mathbf{x}_1 upon \mathcal{S}_2 is located at

$$\check{\mathbf{x}} = \mathbf{x}_1 + r' \frac{\mathbf{x}_1 - \mathbf{x}_2}{\|\mathbf{x}_1 - \mathbf{x}_2\|_2} , \quad (11)$$

where r' is defined by Equation 6. Thus any improved radius of certification $r'' > r'$ is only achievable if $B_P(\mathbf{x}_3, r_3)$ satisfies $\check{\mathbf{x}} \in B_P(\mathbf{x}_3, r_3)$ and Equation 8. Then by symmetry, r'' is the maximally achievable radius of certification if Equation 9 hold and if \mathbf{x}_3 is defined by Equation 10. \square

While finding some \mathbf{x}_3 satisfying Equations 8 and 10 is trivial, proving Equation 9 would require an exhaustive search of the input space $[0, 1]^d$. However, even in the absence of such a search, Equation 10 still provides the framework for a simple search for \mathbf{x}_3 , which follows Figure 1b.

Lemma 3.4 (Certification from two eccentric hyperspheres). *If \mathbf{x}_3 is defined by Equation 10 in a fashion that satisfies Equation 8 then an updated certification can be achieved in terms of some $\mathbf{x}_3(s)$ defined by Equation 10 by way of*

$$\begin{aligned} r'' &= \max_{s \in [0, 1]} \sqrt{\frac{d_2(r_3^2 - d_3^2) + d_3(r_2^2 - d_2^2)}{d_2 + d_3}} \text{ where} \\ d_2 &= \|\mathbf{x}_2 - \mathbf{x}_1\| \quad d_3 = \|\mathbf{x}_3(s) - \mathbf{x}_1\| \quad r_3 = \frac{\sigma}{2} (\Phi^{-1}(E_0[\mathbf{x}_3(s)]) - \Phi^{-1}(E_1[\mathbf{x}_3(s)])) . \end{aligned} \quad (12)$$

If Equation 9 holds, then this is the largest achievable certification for $n = 3$.

Proof. By symmetry we can define the arbitrary rotational mapping $f : \mathcal{R}^d \rightarrow \mathcal{R}^d$ from $\mathbf{x}_i \mapsto \mathbf{y}_i$ by way of $\mathbf{y}_i = f(\mathbf{x}_i - \mathbf{x}_1)$, subject to the condition

$$y_{i,j} \neq 0 \text{ for } i \in \{1, 2\} \text{ and } \forall j \neq k, \text{ for some } k \text{ such that } j, k \in \{1, 2, \dots, d\} \quad (13)$$

then the intersection of the hyperspheres centred about \mathbf{x}_2 and \mathbf{x}_3 occurs at

$$\begin{aligned} r_3^2 - r_2^2 &= \|\mathbf{y} - \mathbf{y}_3\|^2 - \|\mathbf{y} - \mathbf{y}_2\|^2 \\ &= 2y_{2,k}(d_2 + d_3) + d_3^2 - d_2^2 \\ 2y_{2,k} &= \frac{r_3^2 - r_2^2 + d_2^2 - d_3^2}{d_2 + d_3} . \end{aligned} \quad (14)$$

This is a consequence of our mapping $y = f(\mathbf{x} - \mathbf{x}_1)$ preserving distances under rotation, giving that $y_{2,k} = \|\mathbf{x}_2 - \mathbf{x}_1\| = d_2$, and with the equivalent also holding for $y_{3,k}$.

As a consequence of our choice of coordinate system, it follows that $r'' = \|\mathbf{y}\|$ and

$$\begin{aligned} (r'')^2 &= \|\mathbf{y} - \mathbf{y}_2\|^2 + 2y_{2,k}d_2 - d_2^2 \\ &= r_2^2 - d_2^2 + \frac{d_2r_3^2 - d_2r_2^2 + d_2d_2^2 - d_2d_3^2}{d_2 + d_3} \end{aligned} \quad (15)$$

which is an equivalence to Equation (12). \square

While Equation 7 holds for any $n \geq 2$, the certification radius beyond $n = 3$ cannot be enhanced by adding any one single additional hypersphere without contradicting Lemma 3.4. This is a result of \mathbf{S}_3 being a $(d-1)$ -dimensional manifold in \mathcal{R}^d , the entirety of which must be enclosed to improve the certification. An example of this can be seen with the two equidistant intersections between \mathcal{S}_2 (in Red) and \mathcal{S}_3 (in Black) in Figure 1b. While multiple spheres could be constructed to completely enclose \mathbf{S}_3 , the number required grows exponentially with d due to the sphere packing kissing number problem [9]. This growth in complexity makes adding additional spheres beyond $n = 3$ infeasible. Further details of this are contained within Appendix A.2.

3.3 Boundary treatments

Without loss of performance or accuracy, we can freely scale the inputs of neural networks such that $\mathbf{x}_1 \in [0, 1]^d$. However in the majority of cases a subset of $B_P(\mathbf{x}_1, L_1)$ will exist outside $[0, 1]^d$. While this observation is trivially true, it has no influence on the radius of certification achieved by Equation 3 due to the symmetry of $B_P(\mathbf{x}_1, r)$. However, the asymmetric nature of $B_P(\mathbf{x}_2, r_2)$ about \mathbf{x}_1 guarantees that if $B_P(\mathbf{x}_2, r_2)$ exceeds $[0, 1]^d$, then the closest point to \mathbf{x}_1 within the feasible domain must have an associated distance $\hat{r} > r'$, as is demonstrated within Figure 1c. This allows us to make the following observation about improving the feasible radius of certification.

Lemma 3.5 (Boundary Certifications by way of Eccentric Circles). *The eccentricity of $B_P(\mathbf{x}_2, L_2)$ as a bounding region about \mathbf{x}_1 , and the potential for a subset of $B_P(\mathbf{x}_2, L_2)$ to exist outside the feasible space for instances allows us to construct an updated region of certification where*

$$\begin{aligned} \hat{r} &= \max_{k \in \{1, \dots, d\}} \mathbb{1} [r_2^2 - (x_{2,k} - z_k)^2 \geq 0] \times \\ &\quad \sqrt{(z_k - x_{1,k})^2 + \left(\sqrt{r_2^2 - (z_k - x_{2,k})^2} - \sqrt{\|\mathbf{x}_2 - \mathbf{x}_1\|^2 - (x_{2,k} - x_{1,k})^2} \right)^2} \quad (16) \end{aligned}$$

where $z_k = \begin{cases} 0 & \text{if } x_{1,k} < 0.5 \\ 1 & \text{if } x_{1,k} > 0.5 \end{cases}$,

where $\mathbb{1}$ is an indicator function acting upon its operator.

Proof. In contrast to the prior proof, for this problem we retain the coordinate system of the input space. To support this, we introduce the notation that $\mathbf{x}_n = \{x_{n,1}, x_{n,2}, \dots, x_{n,d}\}$. If we let $x_k \in \{0, 1\}$, then the intersection between $B_P(\mathbf{x}_2, L_2)$ and the bounding surface in dimension k creates a bounding hypersphere of the form

$$\sum_{i=1, i \neq k}^d (x_i - x_{2,i})^2 = r_2^2 - (x_k - x_{2,k})^2. \quad (17)$$

which yields an effective radius $\tilde{r}_2 = \sqrt{r_2^2 - (x_k - x_{2,k})^2}$.

By denoting the projection of \mathbf{x}_1 and \mathbf{x}_2 onto the bounding hyperplane in the k -th dimension as $\widetilde{\mathbf{x}}_1$ and $\widetilde{\mathbf{x}}_2$, then the distance from \mathbf{x}_1 to Equation (17) must take the form

$$\begin{aligned} \hat{r}_k &= \sqrt{\|\widetilde{\mathbf{x}}_1 - \mathbf{x}_1\|^2 + (\tilde{r}_2 - \|\widetilde{\mathbf{x}}_2 - \widetilde{\mathbf{x}}_1\|)^2} \\ &= \sqrt{(z_k - x_{1,k})^2 + \left(\sqrt{r_2^2 - (z_k - x_{2,k})^2} - \sqrt{\|\mathbf{x}_2 - \mathbf{x}_1\|^2 - (x_{2,k} - x_{1,k})^2} \right)^2}. \quad (18) \end{aligned}$$

Algorithm 1 Single Bubble Loop.

```

1: Input: data  $\mathbf{x}$ , samples  $N$ , iterations  $M$ , true-label  $i$ 
2: for  $1$  to  $M$  do
3:    $\check{E}_0, \hat{E}_1, L_2, j = \text{Algorithm 2}(\mathbf{x}' + \mathcal{N}(0, \sigma^2 \mathcal{I}_N), N, \sigma)$ 
4:   if  $j = i$  then
5:      $r' = L_2 - \|\mathbf{x}' - \mathbf{x}\|$ 
6:     if  $r' > r'_o$  then
7:        $r'_o = r'$ 
8:     end if
9:      $\mathbf{x}' = \mathbf{x}' \pm \gamma \frac{\nabla_{\mathbf{x}'} r'}{\|\nabla_{\mathbf{x}'} r'\|}$   $\{\gamma \text{ calculated by Barzilai-Borwein [1]. Positive branch is selected if } j = i, \text{ otherwise the negative branch brings } \mathbf{x}' \text{ towards the region in which } j = i.\}$ 
10:   end if
11: end for

```

By imposing that $z_k = 1$ when the k -th component of \mathbf{x}_1 is greater than 0.5, and 0 otherwise, it follows that $\max_{k \in \{0, 1, \dots, d\}} z_k$ must be an improved radius of certification. \square

3.4 Algorithms

To demonstrate how the above certification approaches can be applied in practice, Algorithm 1 demonstrates the application of Equation (5) through a simple, gradient based solver. Such a solver is highly applicable for solving such problems, due to the inherent smoothing nature of randomised smoothing being applicable both to the function space and its derivatives. To implement the multiple transitivity based approach of Section 3.2, Algorithm 1 can trivially be adapted to evaluate derivatives with respect to Equation (12). The boundary treatment of Section 3.3 does not require any additional calculations, but instead is simply the result of applying Equation (16) to the output of Algorithm 1.

4 Extracting gradient information from non-differentiable functions

Implementing the aforementioned process requires the ability to evaluate the gradient of the class expectations. This is problematic, as each class expectation is described in terms of a finite sum of non-differentiable indicator functions, as is seen in Equation (2). Within this work we have implemented two mechanisms to circumvent these conditions. The first substitutes the arg max operation with a Gumbel-Softmax [15]. In doing so, the class expectations are rendered differentiable.

The second approach involves recasting the Monte-Carlo estimators as integrals of the form

$$E[\arg \max f_\theta(\mathbf{x}) = k] = \int \mathbb{1}[\arg \max f_\theta(\mathbf{y}) = k] \omega(\mathbf{y}, \mathbf{x}) d\mathbf{y}, \quad (19)$$

where $\omega(\mathbf{y}, \mathbf{x})$ is the multivariate-Normal probability distribution centred around \mathbf{x} . This formalism, and the symmetry of the underlying space allows for the construction of undifferentiable gradients by

$$\begin{aligned}
\nabla_{\mathbf{x}} E[\arg \max f_\theta(\mathbf{x}) = k] &= \nabla_{\mathbf{x}} \int \mathbb{1}[\arg \max f_\theta(\mathbf{y}) = k] \omega(\mathbf{y}, \mathbf{x}) d\mathbf{y} \\
&\approx \int \mathbb{1}[\arg \max f_\theta(\mathbf{y}) = k] \nabla_{\mathbf{x}} \omega(\mathbf{y}, \mathbf{x}) d\mathbf{y} \\
&= \frac{1}{\sigma^2} \int \mathbb{1}[\arg \max f_\theta(\mathbf{y}) = k] (\mathbf{y} - \mathbf{x}) \omega(\mathbf{y}, \mathbf{x}) d\mathbf{y} \\
&\approx \frac{1}{N\sigma^2} \sum_{i=1}^N \mathbb{1}[\arg \max f_\theta(\mathbf{x}_i) = k] (\mathbf{x}_i - \mathbf{x}) \\
&\quad \text{where } \mathbf{x}_i = \mathbf{x} + \mathcal{N}(0, \sigma^2).
\end{aligned} \quad (20)$$

While this derivation is novel, the resultant gradient operator reflects those seen in prior works [33]. It is important to note that such a sampling process is inherently noisy, and it has previously suggested that the underlying uncertainty scales with the input dimensionality [27].

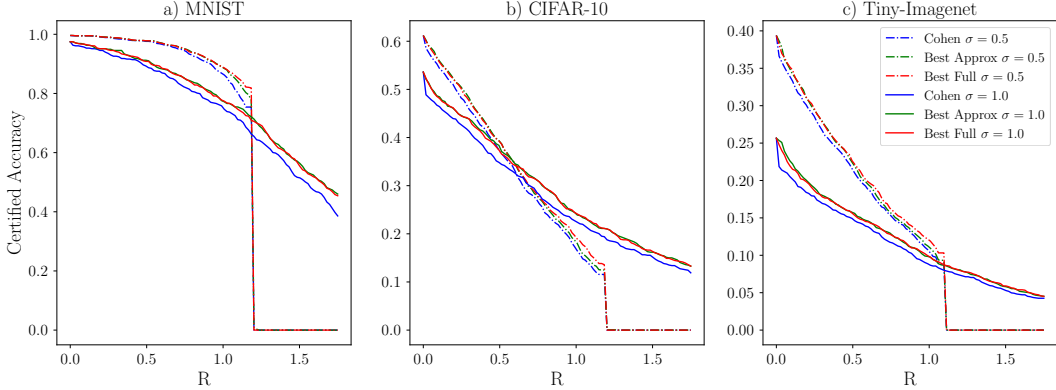


Figure 2: The Certified Accuracy: the proportion of samples correctly predicted and with a certified radius greater than R . Blue represents Cohen, while Green and Red respectively represent the best sub-variant utilising either the Approximate or Full derivative approaches. Dashed lines for $\sigma = 0.5$, solid lines for $\sigma = 1.0$.

The relative performance of these two approaches—respectively labelled ‘Approximate’ and ‘Full’ for the above approach and the Gumbel-Softmax approaches—will be tested in the following section. For the case of the double transitivity of Section 3.2 our experiments suggest that uncertainty in the analytic derivatives produces deleterious results. As such derivatives for the multiple transitivity approach are exclusively considered through autograd for both the Full and Approximate methods.

5 Experiments

Configuration To evaluate the performance of our proposed certification improvements, we considered the certified radius produced for MNIST [19], CIFAR-10 [18], and Tiny-Imagenet [16], the latter of these is a 200-class variant of Imagenet [43] which downsamples images to $3 \times 60 \times 60$. All datasets were modelled using the Resnet18 architecture in PyTorch [32], with Tiny-Imagenet also utilising 2D adaptive average pooling. For both MNIST and CIFAR-10, our experimentation utilised a single NVIDIA P100 GPU core with 12 GB of GPU RAM, with expectations estimated over 1500 samples. Training employed Cross Entropy loss with a batch size of 128 over 50 epochs. Each epoch involved every training example was perturbed with a single perturbation drawn from $\mathcal{N}(0, \sigma^2)$, which was added prior to normalisation. Parameter optimisation was performed with Adam [17], with the learning rate set as 0.001. Tiny-Imagenet training and evaluation utilised 3 P100 GPU’s and utilised 1000 samples. Training occurred using SGD over 80 epochs, with a starting learning rate of 0.1, decreasing by a factor of 10 after 30 and 60 epochs, and momentum set to 0.9.

The full code to implement our experiments can be found at <https://github.com/andrew-cullen/DoubleBubble>.

Certified accuracy To explore the performance advantage provided by our technique, we begin by considering the performance of Cohen *et al.* against the best of our approaches using both the approximate and full derivatives, as seen in Figure 2. While there are only minor differences between the two derivative approaches, there are clear regions of out performance relative to Cohen across all tested datasets. The proportion of this increase appears to be tied to the semantic complexity of the underlying dataset, with decreases in predictive accuracy (visible at $R = 0$) appearing to elicit greater percentage changes in the achieved certified radius, as evidenced by the results for Tiny-Imagenet.

Semantic complexity drives a decrease in the overall confidence of models, inducing a decrease in the separation between the highest class expectations E_0 and E_1 . While this process shrinks the achievable certified radius, a higher E_1 provides more information to inform our gradient based search process, allowing for the identification of larger certifications. This property would suggest that samples with a larger R would exhibit a decreased difference between our techniques and that of Cohen *et al.* would decrease, as smaller values of E_1 provide less search information. However, it appears that singularities in the derivatives of $\Phi^{-1}[E]$ as $E \rightarrow \{0, 1\}$ counteract the decreased

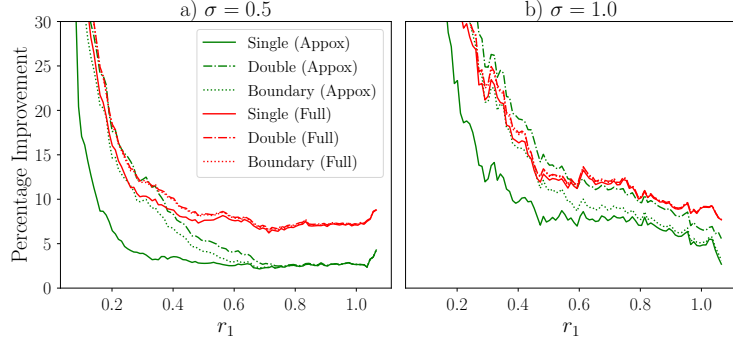


Figure 3: Percentage improvement in the Certified Radius of Tiny-Imagenet instances relative to Cohen *et al.*, for varying r . This measure presents the median improvement over $[r - 0.075, r + 0.075]$. Equivalent figures for MNIST and CIFAR-10 are found in Appendix A.3

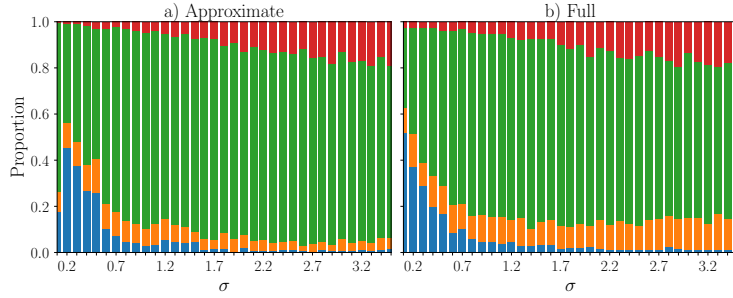


Figure 4: Proportion of correctly predicted instances for which each approach yields the highest certification for Tiny-Imagenet. Red, Green, and Orange represent the boundary treatment, Double transitivity, and Single transitivity, with both ties Cohen *et al.* in Blue. MNIST and CIFAR-10 results can be seen in Appendix A.3

information provided by the second highest class, leading to the contradictory performance best observed in the MNIST experiments of Figure 2 at $\sigma = 0.5$.

Rather than strictly considering the best performing of the Approximate and Full solvers, we can also delve into the relative performance of the underlying solvers. Notably there is a moderate increase in the average percentage improvement of Figure 3 between the $\sigma = 0.5$ and $\sigma = 1.0$ cases. This would appear to belie our previous statement regarding larger certifications yielding smaller improvements, due to the asymmetry of class information. However, an equivalent certification for $\sigma = 1.0$ has significantly more information about the second class (due to the multiplicative influence of σ), allowing for greater improvements from our gradient based search. That there is a clear demarcation between the Full and Approximate solver variants reflects the uncertainties introduced by Equation (20). That the approximate technique is still applicable verifies the utility of our approach even when the final layer is a strict arg max function, rather than a Gumbel-Softmax.

The trends in performance across σ are further explored in Figures 4 and 6, the latter of which demonstrates that the median performance improvement increases quasi-linearly with σ . This is driven by both an increase in the performance of the certifications themselves, and in the number of instances able to be certified in an improved fashion. This latter property stems from the smoothing influence of σ , with larger levels of added noise inducing decreases in the difference between the highest class expectations, improving the ability for our search based mechanisms to identify performance improvements. Here increases in the performance of the boundary treatment are correlated with larger radii of certification, due to the multiplicative influence of σ upon Equation (3).

Numerical performance The numerical optimisation process at the core of our certification process inherently induces increases in the computational cost of finding these improved certifications, as

Table 1: Average wall clock time (in seconds) for each computational technique, for a single sample evaluated over 1000 draws under noise.

Dataset	Cohen	Approx.			Full		
		Single	Boundary	Double	Single	Boundary	Double
M	0.08	0.66	0.66	2.94	2.17	2.17	3.97
C-10	0.08	0.76	0.76	3.83	2.08	2.08	4.62
T-I	0.12	1.13	1.13	5.61	2.87	2.86	7.95

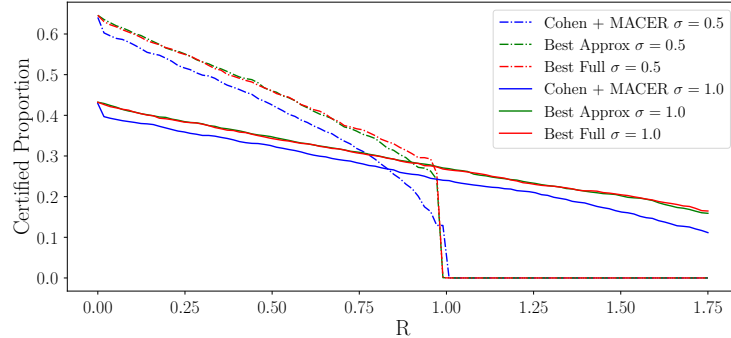


Figure 5: Certified Accuracy comparing the Cohen certification (when trained incorporating MACER) for CIFAR-10, as well as the best sub-variant utilising either the Approximate or Full derivative approaches (also employing MACER). Dashed lines for $\sigma = 0.5$, solid lines for $\sigma = 1.0$.

shown in Table 1. While analytically approximating the derivatives for the first eccentric hypersphere yields a lower certified accuracy, the fact that the corresponding computational cost decreases by a factor of more than 4 emphasises the value of this approach. Interestingly, while the Approximate method does also utilise auto-differentiation for the Double variant, the increase in computational cost from the Single to Double variants is significantly higher than for the Actual approach. This is surprising, as the Approx variant derives smaller values of r' , which should in turn lead to a smaller, easier to navigate search space for r'' . Instead it counter-intuitively appears that a smaller r' induces a search space for r'' which is less convex, and more difficult to converge upon.

Alternative training routines Recent work has considered the potential for enhancing certified robustness by modifying the underlying training regime to incentivise maximising the expectation gap between classes [33]. One such approach is MACER [44], which augments the training time behaviour by considering not just the classification loss, but also the ϵ -robustness loss, which reflects proportion of training samples with robustness above a threshold level. Such a training time modification can increase the average certified radius by 10 – 20%, however doing so does increase the overall training cost by more than an order of magnitude.

When applying Geometrically-Informed Certified Robustness to models trained with MACER, Figure 5 demonstrates that our modifications yield an even more significant improvement than those observed in Figure 2. Under training with MACER, the best performing of our techniques yielded an approximately 4 percentage point increase in the average certification. From this it is clear that while MACER does enhance the certified radii at a sample point, it also induces enough smoothing in the neighbourhood of the sample point to allow transitivity to yield even more significant improvements than are present without MACER.

However, we must emphasise that while such training time modifications do produce consistently larger certifications, doing so requires significantly more computational resources, both in terms of training time and GPU memory, as compared to the more traditional certification training regime. We also emphasise that training with MACER requires a degree of re-engineering. In contrast the training mechanism used for the remainder of this work only requires the addition of noise to samples prior to being passed through the model, and thus imposes significantly fewer engineering considerations.

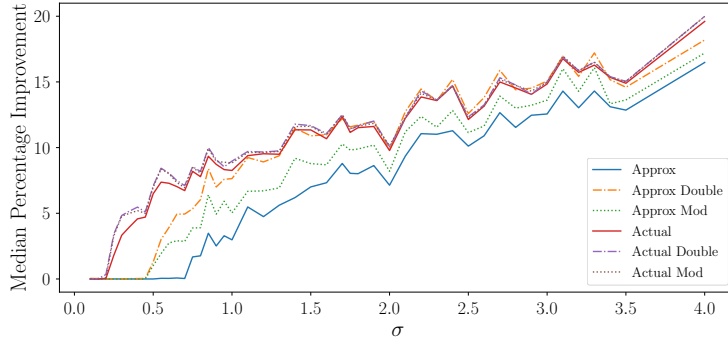


Figure 6: Median percentage improvement in the Certified Radius achieved by each of our approaches relative to Cohen *et al.* for Tiny-Imagenet across the level of additive noise σ . The median was chosen to provide a fair and representative comparison to Cohen *et al.*, that filters out outliers in the percentage improvement when $r \ll 1$.

Limitations While the principles of our Geometrically Informed Certified Robustness are extensible to L_p spaces, our experimental work has so far only considered L_2 -norm bounded perturbations due to the guarantee of best possible certification in this space provided by Cohen *et al.*. Further experimentation could also consider both these general spaces and a broader range of training methods, which have been shown to be able to tighten the achievable radius of certification [24].

We note that enhanced robustness certification have the potential to counter beneficial applications of adversarial attacks, such as those used to promote stylometric privacy [3]. However, we believe this drawbacks is significantly outweighed by the potential for enhanced confidence about models for which adversarial incentives exist.

Finally, we also emphasise that our approach requires M evaluations of the certified robustness, which each require N Monte-Carlo draws, resulting in time- and memory-complexity of $\mathcal{O}(MN)$ and $\mathcal{O}(NS)$ respectively, where S is the size of the output logit vector. With respect to the memory-complexity, this is shared by any randomised smoothing based approach, and could be improved by implementing batching across the Monte-Carlo process. While the time cost can be problematic in some contexts, we emphasise that this framework is both requires both fewer adaptations to the training loop and significantly less training time relative to bound propagation approaches [21, 36]. We believe these costs can be reduced by performing the optimisation stages with $N' < N$ model draws, and by potentially reusing model draws across the iterative process to approach the $\mathcal{O}(N)$ time-complexity of prior randomised smoothing based certifications. Even at present, we believe that the increased computational cost is not intractable, especially for human-in-the-loop certifications.

6 Acknowledgements

This research was undertaken using the LIEF HPC-GPGPU Facility hosted at the University of Melbourne. This Facility was established with the assistance of LIEF Grant LE170100200. This work was also supported in part by the Australian Department of Defence Next Generation Technologies Fund, as part of the CSIRO/Data61 CRP AMLC project. Sarah Erfani is in part supported by Australian Research Council (ARC) Discovery Early Career Researcher Award (DECRA) DE220100680.

7 Conclusions

This work has presented mechanisms that can be exploited to improve achievable levels of certified robustness, based upon exploiting underlying geometric properties of robust neural networks. In doing so our Geometrically Informed Certified Robustness approach has been able to generate certifications that exceed prior guarantees by on average more than 5% at $\sigma = 0.5$, with the percentage increase improving quasi-linearly with σ . Incorporating training time modifications like MACER yields more promising results, with the best performing of our approaches yielding a 4 percentage point increase in the certified proportion at a given radius. Being able to improve upon the size of these guarantees

inherently increases the cost of constructing adversarial attacks against systems leveraging machine learning, especially in the case where the attacker has no ability to observe the size of the robustness certificate.

References

- [1] Jonathan Barzilai and Jonathan M Borwein. Two-Point Step Size Gradient Methods. *IMA Journal of Numerical Analysis*, 8(1):141–148, 1988.
- [2] Battista Biggio, Igino Corona, Davide Maiorca, Blaine Nelson, Nedim Šrndić, Pavel Laskov, Giorgio Giacinto, and Fabio Roli. Evasion Attacks Against Machine Learning at Test Time. In *Joint European Conference on Machine Learning and Knowledge Discovery in Databases*, pages 387–402. Springer, 2013.
- [3] Michael Brennan, Sadia Afroz, and Rachel Greenstadt. Adversarial Stylometry: Circumventing Authorship Recognition to Preserve Privacy and Anonymity. *ACM Transactions on Information and System Security (TISSEC)*, 15(3):1–22, 2012.
- [4] Fabrício Caluza Machado and Fernando Mário de Oliveira Filho. Improving the Semidefinite Programming Bound for the Kissing Number by exploiting Polynomial Symmetry. *Experimental Mathematics*, 27(3):362–369, 2018.
- [5] Nicholas Carlini and David Wagner. Towards Evaluating the Robustness of Neural Networks. In *2017 IEEE Symposium on Security and Privacy (SP)*, pages 39–57. IEEE, 2017.
- [6] Ping-yeh Chiang, Renkun Ni, Ahmed Abdelkader, Chen Zhu, Christoph Studer, and Tom Goldstein. Certified Defenses for Adversarial Patches. *arXiv preprint arXiv:2003.06693*, 2020.
- [7] Wenda Chu, Linyi Li, and Bo Li. TPC: Transformation-Specific Smoothing for Point Cloud Models. *arXiv preprint arXiv:2201.12733*, 2022.
- [8] Jeremy Cohen, Elan Rosenfeld, and Zico Kolter. Certified Adversarial Robustness via Randomized Smoothing. In *International Conference on Machine Learning*, pages 1310–1320. PMLR, 2019.
- [9] HSM Coxeter. An Upper Bound for the Number of Equal Non-Overlapping Spheres that can Touch Another. In *Convexity: Proceedings of the Seventh Symposium in Pure Mathematics of the American Mathematical Society*, volume 7, page 53. American Mathematical Soc., 1963.
- [10] Yinpeng Dong, Fangzhou Liao, Tianyu Pang, Hang Su, Jun Zhu, Xiaolin Hu, and Jianguo Li. Boosting Adversarial Attacks with Momentum. In *Proceedings of the IEEE Conference on Computer Vision and Pattern Recognition*, pages 9185–9193, 2018.
- [11] Cynthia Dwork, Frank McSherry, Kobbi Nissim, and Adam Smith. Calibrating Noise to Sensitivity in Private Data Analysis. In *Theory of Cryptography Conference*, pages 265–284. Springer, 2006.
- [12] Justin Gilmer, Ryan P Adams, Ian Goodfellow, David Andersen, and George E Dahl. Motivating the Rules Of The Game for Adversarial Example Research. *arXiv preprint arXiv:1807.06732*, 2018.
- [13] Ian J Goodfellow, Jonathon Shlens, and Christian Szegedy. Explaining and Harnessing Adversarial Examples. *arXiv preprint arXiv:1412.6572*, 2014.
- [14] Leo A Goodman. On Simultaneous Confidence Intervals for Multinomial Proportions. *Technometrics*, 7(2):247–254, 1965.
- [15] Eric Jang, Shixiang Gu, and Ben Poole. Categorical Reparameterization with Gumbel-Softmax. *arXiv preprint arXiv:1611.01144*, 2016.
- [16] Justin Johnson, Fei-Fei Li, and Andrej Karpathy. Tiny ImageNet Visual Recognition Challenge, Accessed 2022-01-10.
- [17] Diederik P Kingma and Jimmy Ba. Adam: A Method for Stochastic Optimization. *arXiv preprint arXiv:1412.6980*, 2014.
- [18] Alex Krizhevsky, Geoffrey Hinton, et al. Learning Multiple Layers of Features from Tiny Images. Technical report, University of Toronto, 2009.
- [19] Yann LeCun, Léon Bottou, Yoshua Bengio, and Patrick Haffner. Gradient-Based Learning Applied to Document Recognition. *Proceedings of the IEEE*, 86(11):2278–2324, 1998.

[20] Mathias Lecuyer, Vaggelis Atlidakis, Roxana Geambasu, Daniel Hsu, and Suman Jana. Certified Robustness to Adversarial Examples with Differential Privacy. In *2019 IEEE Symposium on Security and Privacy (SP)*, pages 656–672. IEEE, 2019.

[21] Alexander Levine and Soheil Feizi. (de)Randomized Smoothing for Certifiable Defense against Patch Attacks. *Advances in Neural Information Processing Systems*, 33:6465–6475, 2020.

[22] Bai Li, Changyou Chen, Wenlin Wang, and Lawrence Carin. Certified Adversarial Robustness with Additive Noise. In *Advances in Neural Information Processing Systems*, pages 9459–9469, 2019.

[23] Linyi Li, Maurice Weber, Xiaojun Xu, Luka Rimanic, Bhavya Kailkhura, Tao Xie, Ce Zhang, and Bo Li. TSS: Transformation-Specific Smoothing for Robustness Certification. In *Proceedings of the 2021 ACM SIGSAC Conference on Computer and Communications Security*, pages 535–557, 2021.

[24] Linyi Li, Jiawei Zhang, Tao Xie, and Bo Li. Double Sampling Randomized Smoothing. *arXiv preprint arXiv:2206.07912*, 2022.

[25] Zhaoyang Lyu, Minghao Guo, Tong Wu, Guodong Xu, Kehuan Zhang, and Dahua Lin. Towards Evaluating and Training Rerifiably Robust Neural Networks. In *Proceedings of the IEEE/CVF Conference on Computer Vision and Pattern Recognition*, pages 4308–4317, 2021.

[26] Matthew Mirman, Timon Gehr, and Martin Vechev. Differentiable Abstract Interpretation for Provably Robust Neural Networks. In *International Conference on Machine Learning*, pages 3578–3586. PMLR, 2018.

[27] Jeet Mohapatra, Ching-Yun Ko, Tsui-Wei Weng, Pin-Yu Chen, Sijia Liu, and Luca Daniel. Higher-Order Certification for Randomized Smoothing. *Advances in Neural Information Processing Systems*, 33:4501–4511, 2020.

[28] Jeet Mohapatra, Tsui-Wei Weng, Pin-Yu Chen, Sijia Liu, and Luca Daniel. Towards Verifying Robustness of Neural Networks against a family of Semantic Perturbations. In *Proceedings of the IEEE/CVF Conference on Computer Vision and Pattern Recognition*, pages 244–252, 2020.

[29] Oleg R Musin. The Kissing Number in Four Dimensions. *Annals of Mathematics*, pages 1–32, 2008.

[30] Andrew M Odlyzko and Neil JA Sloane. New Bounds on the number of Unit Spheres that Can Touch a Unit Sphere in n Dimensions. *Journal of Combinatorial Theory, Series A*, 26(2):210–214, 1979.

[31] Nicolas Papernot, Patrick McDaniel, Ian Goodfellow, Somesh Jha, Z Berkay Celik, and Ananthram Swami. Practical Black-Box Attacks against Machine Learning. In *Proceedings of the 2017 ACM on Asia Conference on Computer and Communications Security*, pages 506–519, 2017.

[32] Adam Paszke, Sam Gross, Francisco Massa, Adam Lerer, James Bradbury, Gregory Chanan, Trevor Killeen, Zeming Lin, Natalia Gimelshein, Luca Antiga, Alban Desmaison, Andreas Kopf, Edward Yang, Zachary DeVito, Martin Raison, Alykhan Tejani, Sasank Chilamkurthy, Benoit Steiner, Lu Fang, Junjie Bai, and Soumith Chintala. Pytorch: An Imperative Style, High-Performance Deep Learning Library. In H. Wallach, H. Larochelle, A. Beygelzimer, F. d’Alché Buc, E. Fox, and R. Garnett, editors, *Advances in Neural Information Processing Systems 32*, pages 8024–8035. Curran Associates, Inc., 2019.

[33] Hadi Salman, Jerry Li, Ilya Razenshteyn, Pengchuan Zhang, Huan Zhang, Sebastien Bubeck, and Greg Yang. Provably Robust Deep Learning via Adversarially Trained Smoothed Classifiers. In *Advances in Neural Information Processing Systems*, 2019.

[34] Hadi Salman, Greg Yang, Huan Zhang, Cho-Jui Hsieh, and Pengchuan Zhang. A Convex Relaxation Barrier to Tight Robustness Verification of Neural Networks. In *Advances in Neural Information Processing Systems*, 2019.

[35] Kurt Schütte and Bartel Leendert van der Waerden. Das Problem der Dreizehn Kugeln. *Mathematische Annalen*, 125(1):325–334, 1952.

[36] Zhouxing Shi, Yihan Wang, Huan Zhang, Jinfeng Yi, and Cho-Jui Hsieh. Fast Certified Robust Training with Short Warmup. *Advances in Neural Information Processing Systems*, 34:18335–18349, 2021.

- [37] Gagandeep Singh, Timon Gehr, Markus Püschel, and Martin Vechev. An Abstract Domain for Certifying Neural Networks. *Proceedings of the ACM on Programming Languages*, 3(POPL):1–30, 2019.
- [38] Cristina P Sison and Joseph Glaz. Simultaneous Confidence Intervals and Sample Size Determination for Multinomial Proportions. *Journal of the American Statistical Association*, 90(429):366–369, 1995.
- [39] David J Smith and Mavina K Vamanamurthy. How Small is a Unit Ball? *Mathematics Magazine*, 62(2):101–107, 1989.
- [40] Shiqi Wang, Huan Zhang, Kaidi Xu, Xue Lin, Suman Jana, Cho-Jui Hsieh, and J Zico Kolter. Beta-CROWN: Efficient Bound Propagation with Per-Neuron Split Constraints for Neural Network Robustness Verification. *Advances in Neural Information Processing Systems*, 34, 2021.
- [41] Lily Weng, Huan Zhang, Hongge Chen, Zhao Song, Cho-Jui Hsieh, Luca Daniel, Duane Boning, and Inderjit Dhillon. Towards Fast Computation of Certified Robustness for ReLU Networks. In *International Conference on Machine Learning*, pages 5276–5285. PMLR, 2018.
- [42] Kaidi Xu, Zhouxing Shi, Huan Zhang, Yihan Wang, Kai-Wei Chang, Minlie Huang, Bhavya Kailkhura, Xue Lin, and Cho-Jui Hsieh. Automatic Perturbation Analysis for Scalable Certified Robustness and Beyond. *Advances in Neural Information Processing Systems*, 33, 2020.
- [43] Kaiyu Yang, Jacqueline Yau, Li Fei-Fei, Jia Deng, and Olga Russakovsky. A Study of Face Obfuscation in Imagenet. *arXiv preprint arXiv:2103.06191*, 2021.
- [44] Runtian Zhai, Chen Dan, Di He, Huan Zhang, Boqing Gong, Pradeep Ravikumar, Cho-Jui Hsieh, and Liwei Wang. MACER: Attack-free and scalable robust training via maximizing certified radius. In *International Conference on Learning Representations*, 2020.
- [45] Huan Zhang, Tsui-Wei Weng, Pin-Yu Chen, Cho-Jui Hsieh, and Luca Daniel. Efficient Neural Network Robustness Certification with General Activation Functions. In S. Bengio, H. Wallach, H. Larochelle, K. Grauman, N. Cesa-Bianchi, and R. Garnett, editors, *Advances in Neural Information Processing Systems 31*, pages 4939–4948. Curran Associates, Inc., 2018.
- [46] Huan Zhang, Tsui-Wei Weng, Pin-Yu Chen, Cho-Jui Hsieh, and Luca Daniel. Efficient Neural Network Robustness Certification with General Activation Functions. In *Neural Information Processing Systems (NeurIPS)*, 2018.

Algorithm 2 Class prediction and certification, as required for Algorithm 1

```

1: Input: Perturbed data  $\mathbf{x}'$ , samples  $N$ , level of added noise  $\sigma$ 
2:  $\mathbf{y} = \mathbf{0}$ 
3: for  $i = 1:N$  do
4:    $y_j = y_j + 1$  if  $GS(f_\theta(\mathbf{x}' + \mathcal{N}(0, \sigma^2))) = j$  {Here  $GS$  is the Gumbel-Softmax}
5: end for
6:  $\mathbf{y} = \frac{1}{N}\mathbf{y}$ 
7:  $z_0, z_1 = \text{topk}(\mathbf{y}, k = 2)$  {topk is used as it is differentiable,  $z_0 > z_1$ }
8:  $\check{E}_0, \hat{E}_1 = \text{lowerbound}(\mathbf{y}, z_0), \text{upperbound}(\mathbf{y}, z_1)$  {Calculated by way of Goodman et al. [14]}
9:  $R = \frac{\sigma}{2} \left( \Phi^{-1}(\check{E}_0) - \Phi^{-1}(\hat{E}_1) \right)$ 
10: return  $\check{E}_0, \hat{E}_1, R, j$ 

```

A Appendix

A.1 Algorithmic details

Algorithm 2 supports Algorithm 1 by demonstrating how the class prediction and expectations are calculated. Of note are two minor changes from prior implementations of this certification regime. The first is the addition of the Gumbel-Softmax on line 4, although this step is only required for the ‘Full’ derivative approach. In contrast the ‘Approximate’ techniques able to circumvent this limitation and can be applied directly to the case where the class election is determined by an $\arg \max$.

The second difference to prior works is the calculation of the lower and upper bounds on z_0 and z_1 on line 8. Our initial testing revealed that when we employed either Sisson-Glaz [38] or Goodman *et al.* [14] to estimate the multivariate class uncertainties, some Tiny-Imagenet samples devoted more than 95% of their computational time of the process to evaluating the confidence intervals, significantly outweighing even the costly process of model sampling. Further investigation revealed that this was occurring when there were a significant number of classes reporting counts of approximately 0, the likelihood for which was higher in Tiny-Imagenet due to the increased class count relative to MNIST and CIFAR-10. To resolve this, we coalesced all classes where $y_j < 5$ into one single meta-class with an associated class-count $y' = \max(5, \sum_{y_j < 5} y_j)$, which conforms with the requirements of Goodman *et al.* [14] that all class counts must be greater than 5. Our testing demonstrated that while this process slightly decreased the resulting radius of certification (due to small changes in z_0 and z_1), the associated decrease in computational time was significant enough to justify this modification.

We also note that all the experiments contained within this work have been conducted against publically released datasets with established licenses. MNIST exists under a GNU v3.0 license; CIFAR-10 employs a MIT license; and Imagenet employs a BSD 3-Clause license.

A.2 Ramifications of the dimensionality for $n > 3$

To improve the achieved certification in the case $n > 3$, the added set of hyperspheres must fully enclose the $(d - 1)$ -dimensional manifold that marks the intersection between \mathcal{S}_2 and \mathcal{S}_3 . In two-dimensions—as is used in the exemplar Figure 1a—this intersection takes the form of two points. If Lemma’s 3.3 and 3.4 are to hold, then encompassing $\mathcal{S}_2 \cap \mathcal{S}_3$ will require two additional certification hyperspheres to be identified.

In the case where $d = 3$, the intersection between these two hyperspheres is the boundary of the circle (equivalent to a $d = 2$ hypersphere) with radius

$$\tilde{r} = \sqrt{r_2^2 - \frac{\|\mathbf{x}_3 - \mathbf{x}_2\|_2 - r_3^2 + r_2^2}{2\|\mathbf{x}_3 - \mathbf{x}_2\|_2}}. \quad (21)$$

Thus any set of spheres $\{\mathcal{S}_2, \mathcal{S}_3, \dots, \mathcal{S}_n\}$ must uniformly cover all points on the boundary of this surface if we seek to improve the achieved certification.

To provide an indicative example of how the complexity of the region that must be encircled grows with the underlying dimensionality, we now consider some properties of hyperspheres. In higher

dimensions, prior work [39] has demonstrated that the volume contained within a d -dimensional hypersphere can be expressed as

$$V_d(\tilde{r}) = \frac{\tilde{r}^d \pi^{d/2}}{\Gamma\left(\frac{d}{2} + 1\right)}, \quad (22)$$

with an associated surface area of

$$\begin{aligned} S_d(\tilde{r}) &= \frac{d(V_d(r))}{d(r)} \Big|_{r=\tilde{r}} \\ &= \frac{d\tilde{r}^{d-1} \pi^{d/2}}{\Gamma\left(\frac{d}{2} + 1\right)}. \end{aligned} \quad (23)$$

Thus if S_2 and S_3 are d -dimensional hyperspheres, then their region of intersection would in turn be a $(d-1)$ -dimensional hypersphere, the exterior boundary of which scales with \tilde{r}^{d-2} . While \tilde{r} may be less than 1, it should also be true that any additional spheres would likely have an associated radii less than \tilde{r} . As such there would appear to be a power-law proportionality with respect to $(d-1)$ between the area covered by the intersection manifold and the size of spheres over which we would seek to enclose said manifold. This underscores the complexity of finding a set of hyperspheres to encircle the boundary of $\mathcal{S}_2 \cap \mathcal{S}_3$.

To give further evidence in the growth of complexity, let us consider a unit-hypersphere in \mathcal{R}^d that represents the intersection of two hyperspheres in \mathcal{R}^{d+1} . The task of covering such a hypersphere is similar to that of the sphere packing kissing number $k(d)$ [9], which describes the number of touching-but-not-overlapping unit-hyperspheres that can exist upon the surface of a d -dimensional hypersphere. To date, the kissing number has only been solved for the following dimensions outlined in Table 2, however it has been shown to exhibit exponential growth [4].

Table 2: Known Kissing numbers $k(d)$ for d -dimensional hyperspheres

d	1	2	3	4	8	24
$k(d)$	2	6	12 [35]	24 [29]	240 [30]	196,560 [30]

Within the context of this work, the kissing number must be considered to be a significant underestimate of the number of boundary spheres that would be required to be found, as we must cover all the space around the central sphere (rather than just maximising the number of hyperspheres without intersection), and it is unlikely that the smallest of the set of encircling hyperspheres has the same radius as the region to be encircled. As such, we can be highly confident that the growth in complexity of the task of enclosing the boundary of intersection beyond the set of hyperspheres $\{\mathcal{S}_1, \mathcal{S}_2, \mathcal{S}_3\}$ is exponential.

We must also note that even if it were possible to perform such a bounding operation, the gains in certified radius would be exceedingly minor. If the region of intersection between \mathcal{S}_2 and \mathcal{S}_3 was a hypersphere of radius \tilde{r} , then going from the case where $n = 3$ to $n > 3$ would only increase the certified radius from $\sqrt{(r')^2 + (\tilde{r})^2}$ to $\sqrt{(r')^2 + 9(\tilde{r})^2}$, which is trivial relative to the increase in computational complexity.

A.3 Relative performance for MNIST and CIFAR-10

While Figure 2 presents the best performing certified accuracy, it is important to understand the relative performance of the Single Transitivity, Double Transitivity, and Boundary treatments, in a similar fashion to Figures 3 and 4. In the case of MNIST, while the percentage increases exhibited in Figure 7 as $r_1 \rightarrow 1$ are broadly similar to their Tiny-Imagenet counterpart for the Approximate solver, the difference between those results and the Full derivative treatment is significantly smaller, especially at $\sigma = 1$. This may, in part, be driven by the 1500 samples employed when using MNIST and CIFAR-10, in contrast to 1000 for Tiny-Imagenet, which should decrease the uncertainty of the gradient estimation steps.

However, the fact that this decreased difference in performance holds for CIFAR-10 at $\sigma = 1.0$ but not $\sigma = 0.5$ suggests that the performance difference between the techniques is also dependent upon the semantic complexity of the prediction task. While CIFAR-10 is a more complex predictive

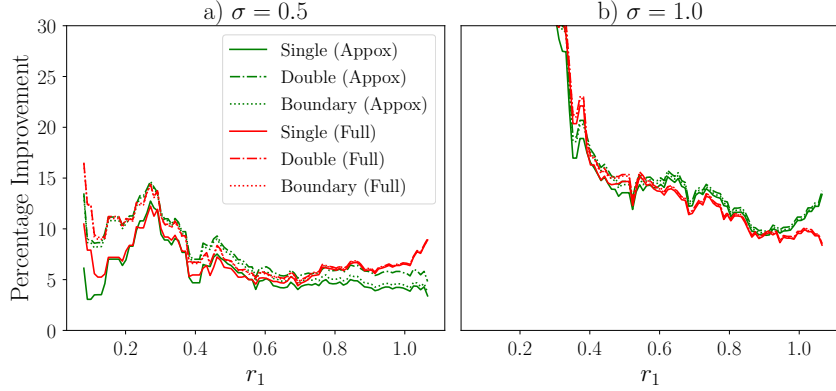


Figure 7: Percentage improvement in the Certified Radius of Tiny-Imagenet instances relative to Cohen *et al.*. for varying r . This measure presents the median improvement over $[r - 0.075, r + 0.075]$. Equivalent figures for Tiny-Imagenet can be seen in Figure 3

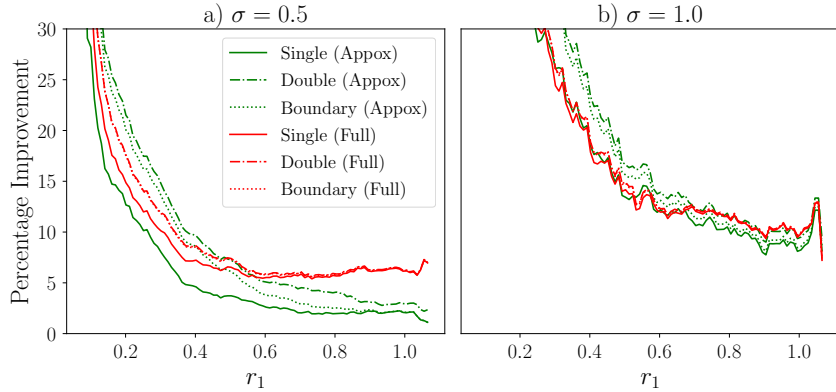


Figure 8: Percentage improvement in the Certified Radius of CIFAR-10 instances relative to Cohen *et al.*. for varying r . This measure presents the median improvement over $[r - 0.075, r + 0.075]$. Equivalent figures for Tiny-Imagenet can be seen in Figure 3

environment than MNIST, which should increase the complexity of the gradient based search routine employed within this work, the increased level of noise at $\sigma = 1.0$ has a smoothing influence that decreases the complexity of the search task, and it would appear that this is the primary driver of the relative under performance of the Approximate derivatives in both Tiny-Imagenet and CIFAR-10 when $\sigma = 0.5$.

When considering the median percentage improvement (relative to Cohen *et al.*) of these techniques, MNIST again reveals interesting properties when we consider Figure 11. When compared to CIFAR-10 and Tiny-Imagenet (in Figures 12 and 6) it becomes apparent that the Approximate approach only produces consistently larger certifications in MNIST. Given the increased uncertainty in the derivatives calculated by the Approximate technique, this would suggest that the approximate solver may be improved by considering common improvements to gradient descent methods like momentum or the addition of calibrated noise.

While MNIST may be the simplest of all the prediction tasks, Figure 9 demonstrates that at low $\sigma < 0.5$ the majority of samples cannot be improved upon by any of the certification enhancements developed within this paper. Given that this does not hold for CIFAR-10 nor Tiny-Imagenet (in Figure 10 and 4 respectively) this would suggest that the potential for Cohen *et al.* to be improved upon in low semantic complexity datasets is smaller. That this behaviour is predominantly seen for small σ also suggests that our initial step size may be too large in these particular cases.

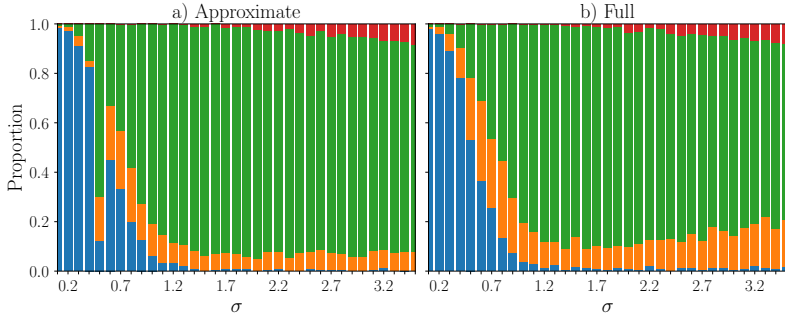


Figure 9: Proportion of correctly predicted instances for which each approach yields the highest certification across σ for MNIST. Red represents the proportion for which the boundary treatment produces the largest certification, with Green, Orange, and Blue representing the same for Double transitivity, Single transitivity, or Cohen *et al.*. While our approaches subsume Cohen, if no other technique is able to improve upon the base certification, we assign the largest certification as having been calculated by Cohen *et al.*.

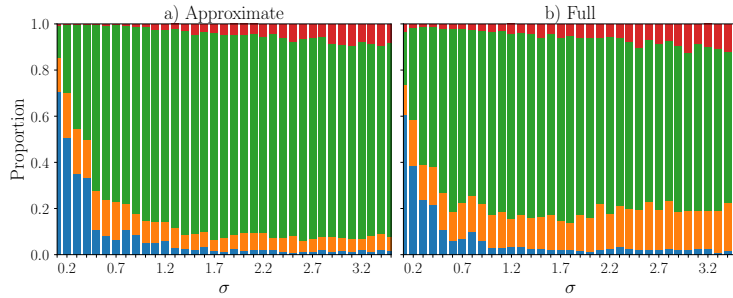


Figure 10: Proportion of correctly predicted instances for which each approach yields the highest certification across σ for CIFAR-10. Red represents the proportion for which the boundary treatment produces the largest certification, with Green, Orange, and Blue representing the same for Double transitivity, Single transitivity, or Cohen *et al.*. While our approaches subsume Cohen, if no other technique is able to improve upon the base certification, we assign the largest certification as having been calculated by Cohen *et al.*.

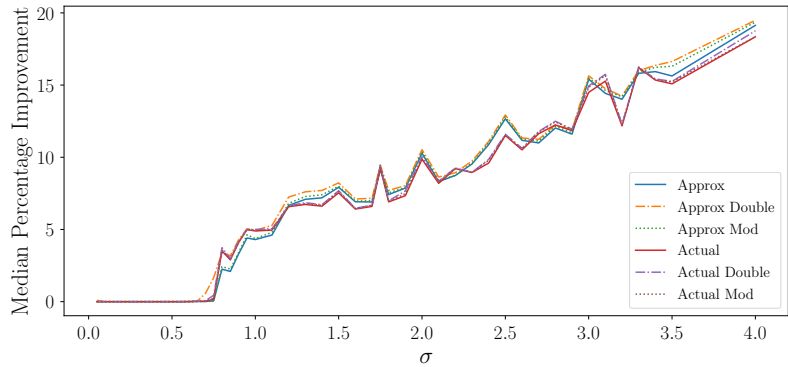


Figure 11: Median percentage improvement of the Certified Robustness achieved by each of our approaches relative to Cohen *et al.* for MNIST across the level of additive noise σ . The median was chosen to provide a fair and representative comparison to Cohen *et al.*, that filters out outliers in the percentage improvement when $r \ll 1$.

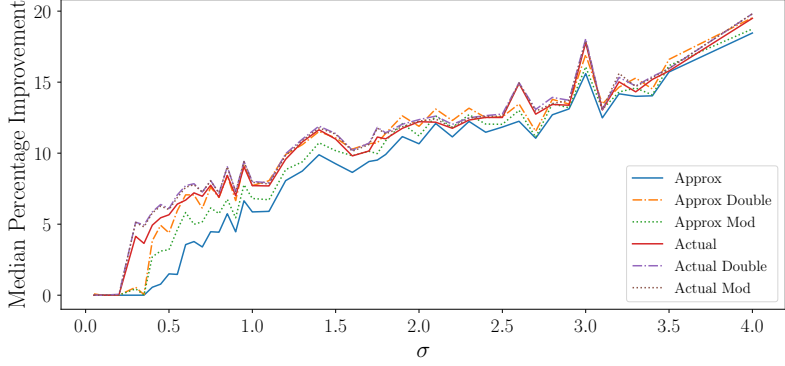


Figure 12: Median percentage improvement of the Certified Robustness achieved by each of our approaches relative to Cohen *et al.* for CIFAR-10 across the level of additive noise σ . The median was chosen to provide a fair and representative comparison to Cohen *et al.*, that filters out outliers in the percentage improvement when $r \ll 1$.

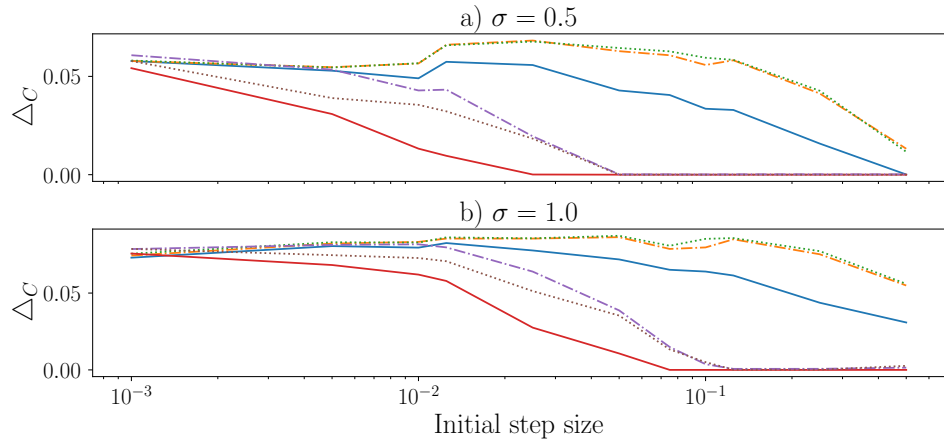


Figure 13: Average delta to the Cohen *et al.* Certified Radius (Δ_C) for CIFAR-10 as a function of the initial step size γ . Here Blue, Green, and Yellow represent the Full Single transitivity, Double transitivity, and Boundary treatments; with Blue, Purple, and Brown representing the same for the Approximate solver.

A.4 Influence of the starting step size

The one heretofore un-considered feature is the influence of the initial step-size γ within Algorithm 1. As is shown in Figures 13 and 14, while the Full solver only exhibits sensitivity to $\gamma > 0.1$, the approximate solvers are far more sensitive, with deleterious performance being observed for $\gamma > 0.01$ in CIFAR-10, and even earlier for Tiny-Imagenet. This is likely due to the added uncertainty in the Approximate derivatives leading to convergence upon local sub-optima in the more semantically complex datasets. Based upon these results, the starting step size was uniformly set to 0.01 for all experiments.

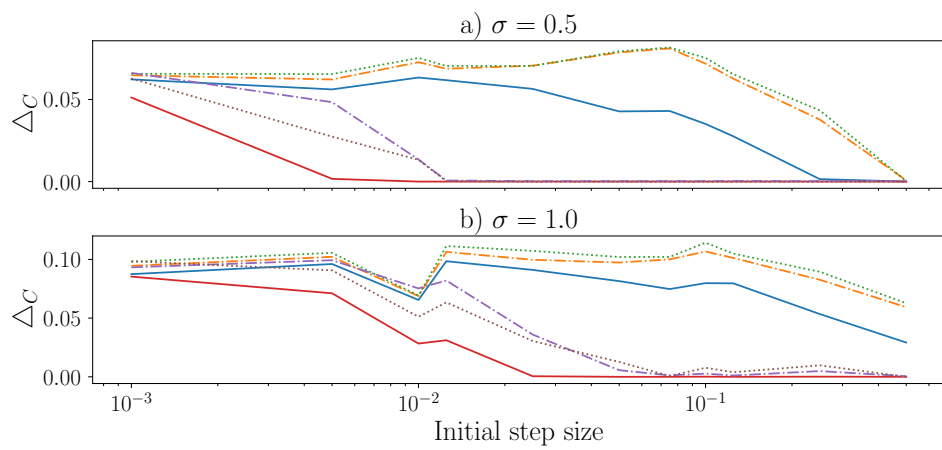


Figure 14: Average delta to the Cohen *et al.* Certified Radius (Δ_C) for Tiny-Imagenet as a function of the initial step size γ . Here Blue, Green, and Yellow represent the Full Single transitivity, Double transitivity, and Boundary treatments; with Blue, Purple, and Brown representing the same for the Approximate solver.